

# A first-principles comparison of the electronic properties of $MgC_yNi_3$ and $ZnC_yNi_3$ alloys

**P. Jiji Thomas Joseph and Prabhakar P. Singh**

Department of Physics, Indian Institute of Technology Bombay, Mumbai India 400076

**Abstract.** First-principles, density-functional-based electronic structure calculations are employed to study the changes in the electronic properties of  $ZnC_yNi_3$  and  $MgC_yNi_3$  using the Korringa-Kohn-Rostoker coherent-potential approximation method in the atomic sphere approximation (KKR-ASA CPA). As a function of decreasing  $C$  at%, we find a steady decrease in the lattice constant and bulk modulus in either alloys. However, the pressure derivative of the bulk modulus displays an opposite trend. Following the Debye model, which relates the pressure derivative of the bulk modulus with the average phonon frequency of the crystal, it can thus be argued that  $ZnCNi_3$  and its disordered alloys possess a different phonon spectra in comparison to its  $MgCNi_3$  counterparts. This is further justified by the marked similarity we find in the electronic structure properties such as the variation in the density of states and the Hopfield parameters calculated for these alloys. The effects on the equation of state parameters and the density of states at the Fermi energy, for partial replacement of  $Mg$  by  $Zn$  are also discussed.

## 1. Introduction

In spite of being iso-structural and iso-valent to the cubic perovskite 8K superconductor  $MgCNi_3$  [1],  $ZnCNi_3$  remains in the normal metal state down to 2K [2]. The specific heat measurements indicate that the absence of superconductivity in  $ZnCNi_3$  may be due to a substantial decrease in the density of states at the Fermi energy  $N(E_F)$  resulting from its relatively low unit cell volume in comparison with  $MgCNi_3$  [2]. However, electronic structure calculations show that the decrease in  $N(E_F)$  is not sizable enough to make  $ZnCNi_3$  non-superconducting [3]. For both  $MgCNi_3$  [4, 5, 6, 7] and  $ZnCNi_3$  [3] the density of states spectra display similar characteristics, particularly in the distribution of electronic states near the Fermi energy  $E_F$ . The electronic states at  $E_F$  are dominated by  $Ni$  3d states with a little admixture of  $C$  2p states. There exists a strong van Hove singularity-like feature just below  $E_F$ , which is primarily derived from the  $Ni$  3d bands.

To account for the lack of superconductivity in  $ZnCNi_3$ , the density-functional based calculations emphasize that the material subjected to the specific heat measurements may be non-stoichiometric in the  $C$  sub-lattice [3]. This would then make it similar to the  $\alpha$ - phase of  $MgCNi_3$ , which has a low unit cell volume and remains non-superconducting [8]. It has been shown earlier that exact  $C$  content in  $MgC_yNi_3$  depends on the nature of synthesis and other experimental conditions [1, 8, 9, 10, 11, 12]. According to Johannes and Pickett [3], the arguments that favor non-stoichiometry are the following: (i) Total energy minimization en-route to equilibrium lattice constant within the local-density approximation (LDA) finds an overestimated value for  $ZnCNi_3$  in comparison with the experimental values. In general, overestimation is not so common in LDA. Meanwhile, when one uses similar technique for  $MgCNi_3$ , the calculations find a slightly underestimated value which is consistent within the limitations of the density-functional theory [4, 13, 14]. (ii) The authors also find  $N(E_F)$  in  $MgCNi_3$  estimated as 13.6 states/Ry atom, while for  $ZnCNi_3$ , under similar approximations, it was found to be 11.01 states/Ry atom. Note that it has been shown both experimentally as well as from first-principles calculations that a decrease in the lattice constant or a decrease in the  $C$  occupancy would lead to a decrease in  $N(E_F)$  [13]. (iii) A decrease in the unit cell dimensions can induce phonon hardening. This is well supported by the experiments which find the Debye temperature approximately 1.6 times higher for  $ZnCNi_3$  in comparison to  $MgCNi_3$ [2].

Earlier synthesis of  $ZnC_yNi_3$  [15, 16, 17] finds the lattice constant to be 6.899 a.u., for which the occupancy in the  $C$  sub-lattice was just 70%. The authors have employed similar preparation technique for  $MgCNi_3$  [15] and have found that the  $C$  occupancy ranges between 0.5-1.25, which is consistent with the recent reports [1, 8, 9, 10, 11, 12, 18]. Lattice constant for  $ZnCNi_3$ , as high as 7.126 a.u. has also been reported elsewhere [19, 20], which then becomes consistent with the recent total energy minimized value using density-functional based methods. Hence, it seems that  $ZnCNi_3$  which was subjected to specific heat experiments [2] may indeed suffer from

non-stoichiometry.

To understand and compare the effects of  $C$  stoichiometry on the structural and electronic properties of  $MgC_yNi_3$  and  $ZnC_yNi_3$ , we carry out a detail study using the Korringa-Kohn-Rostoker (KKR) Green's function method [21, 22] formulated in the atomic sphere approximation (ASA) [23]. For disorder, we employ the coherent-potential approximation (CPA) [24]. Characterization of  $MgC_yNi_3$  and  $ZnC_yNi_3$  with  $0.85 \leq y \leq 1.00$  mainly involves the changes in the equation of state parameters viz., the equilibrium lattice constant, bulk modulus and its pressure derivative. The electronic structure is studied with the help of total and sub-lattice resolved density of states. The propensity of magnetism in these materials is studied with the help of fixed-spin moment method [25] in conjunction with the Landau theory of phase transition [26]. The Hopfield parameter  $\eta$  which generally maps the local "chemical" property of an atom in a crystal is also calculated as suggested by Skriver and Mertig [27], and its variation as a function of lattice constant has also been studied. In general, we find that both  $MgCNi_3$  and  $ZnCNi_3$  display very similar electronic structure. Evidences point that the non-superconducting nature of  $ZnCNi_3$  may be related to the crystal structure characteristics, namely phonon spectra.

## 2. Computational details

The ground state properties of  $MgC_yNi_3$  and  $ZnC_yNi_3$  are calculated using the KKR-ASA-CPA method of alloy theory. For improving alloy energetics, the ASA is corrected by the use of both the muffin-tin correction for the Madelung energy [28] and the multi-pole moment correction to the Madelung potential and energy [29, 30]. These corrections have brought significant improvement in the accuracy of the total energy by taking into account the non-spherical part of polarization effects [31]. The partial waves in the KKR-ASA calculations are expanded up to  $l_{max} = 3$  inside atomic spheres, although the multi-pole moments of the electron density have been determined up to  $l_{max}^M = 6$ , which is used for the multi-pole moment correction to the Madelung energy. In general, the exchange-correlation effects are taken into consideration via the local-density approximation with Perdew and Wang parametrization [32], although a comparison in the equation of state parameters has been made in this work with the generalized gradient approximation (GGA) [33]. The core states have been recalculated after each iteration. The calculations are partially scalar-relativistic in the sense that although the wave functions are non-relativistic, first order perturbation corrections to the energy eigenvalues due to the Darwin and the mass-velocity terms are included. The atomic sphere radii of  $Mg$  ( $Zn$ ),  $C$  and  $Ni$  were kept as 1.404, 0.747, and 0.849 of the Wigner-Seitz radius, respectively. The vacancies in the  $C$  sub-lattice are modeled with the help of empty spheres, and their radius is kept same as that of  $C$  itself. The overlap volume resulting from the blow up of the atomic spheres was less than 15%, which is legitimate within the accuracy of the approximation [34].

The electron-phonon coupling parameter  $\lambda$  can be expressed as  $\eta/M \langle \omega^2 \rangle$ , where

$\eta$  is the Hopfield parameter, expressed as the product of  $N(E_F)$  and the mean square electron-ion matrix element  $\langle I^2 \rangle$ , with  $M$  and  $\langle \omega^2 \rangle$  being the ionic mass and average phonon frequency [35]. However, one may note that the above decomposition of the problem into electronic and phonon contributions is only approximate since in principle  $\langle \omega^2 \rangle$  is also determined by the electronic states. It follows that the Hopfield parameter is the most simple basic quantity which one may obtain from first-principles as suggested by Gaspari and Gyorffy [36]. The latter assumes a rigid muffin-tin approximation (RMTA) in which the potential enclosed by a sphere rigidly moves with the ion and the change in the crystal potential, caused by the displacement, is given by the potential gradient. Within the RMTA the spherically averaged part of the Hopfield parameter may be calculated as,

$$\eta_0 = \frac{2}{N(E_F)} \sum_l (l+1) M_{l,l+1}^2 \frac{N_l(E_F) N_{l+1}(E_F)}{(2l+1)(2l+3)} \quad (1)$$

where  $N(E_F)$  is the total density of state per spin at the Fermi energy, and  $N_l$  the  $l^{\text{th}}$  partial density of state calculated at the Fermi energy  $E_F$ , on the site considered. The term  $M_{l,l+1}$  is the electron-phonon matrix element given as [27],

$$M_{l,l+1} = \int_0^S r^2 R_l \frac{dV}{dr} R_{l+1} dr \quad (2)$$

which are obtained from the gradient of the potential and the radial solutions  $R_l$  and  $R_{l+1}$  of the Schrodinger equation evaluated at  $E_F$ . The special form of the Eqs.1 and 2 stems from the ASA in which the radial wave functions are normalised to unity in the atomic sphere of radius  $S$ , i.e.,  $\int_0^S r^2 R_l^2(r) dr = 1$ . In ASA,  $M_{l,l+1}$  is expressed in terms of logarithmic derivatives  $D_l = r R_l' / R_l$  evaluated at the sphere boundary. Skriver and Mertig derive the expression for  $M_{l,l+1}$  as

$$M_{l,l+1} = \frac{-\phi_l(E_F) \phi_{l+1}(E_F) \times}{\{[D_l - l][D_{l+1} + l + 2] + [E_F - V(S)] S^2\}} \quad (3)$$

where  $V(S)$  is the one-electron potential and  $\phi_l(E_F)$  the sphere boundary amplitude of the  $l$  partial wave evaluated at  $E_F$ .

Numerical estimate to the magnetic energy are carried out using the fixed-spin-moment method [25]. In the fixed-spin-moment method the total energy is obtained for a given magnetization  $M$ , i.e., by fixing the numbers of electrons with up and down spins. In this case, the Fermi energies in the up and down spin bands are not equal to each other because the equilibrium condition would not be satisfied for arbitrary  $M$ . At the equilibrium  $M$  two Fermi energies will coincide with each other. The total magnetic energy becomes minimum or maximum at this value of  $M$ . Note that the two approaches, i.e., the self-consistent, floating-spin-moment method as well as the fixed-spin moment-method are equivalent in the sense that for a given lattice constant the magnetic moment calculated by the standard floating-spin moment approach is the same as the magnetic moment for which the fixed-spin moment total energy has its minimum [37]. In practice, the floating-spin moment approach sometimes runs into some

convergence problem. From experience, to avoid such predicaments in convergence, one may carefully monitor the mixing of the initial and final charges during the iterations and increase the number of  $\mathbf{k}$ - points. Thus, for a better resolution to determine the change in the total energy with respect to the input magnetization, the  $\mathbf{k}$ - mesh had 1771  $\mathbf{k}$ - points in the irreducible wedge of the cubic Brillouin zone.

By the fixed-spin-moment method the difference  $\Delta E(M)$  ( $=E(M) - E(0)$ ) for given values of  $M$  is calculated. The calculated  $\Delta E(M)$  is fitted to the phenomenological Landau equation of phase transition which is given as

$$\Delta E(M) = \sum_{n>0} \frac{1}{2n} a_{2n} M^{2n} \quad (4)$$

for  $n = 3$ , where the sign of the coefficient  $a_{2n}$  for  $n = 1$  determines the nature of the magnetic ground state, i.e.,  $a_2 > 0$  refers to a paramagnetic ground state while  $a_2 < 0$  refers to a ferromagnetic phase. We have applied the approach described above to the study of carbon vacancy in  $MgCNi_3$  [13] and 3d transition-metal- $MgCNi_3$  alloys [14].

### 3. Results and Discussion

#### 3.1. Equation of state

Both X-ray and neutron diffraction techniques unambiguously report  $MgCNi_3$  and  $ZnCNi_3$  as cubic perovskites with their lattice constants determined as 7.201 and 6.918 a.u., respectively. Assuming an underlying rigid cubic lattice, with  $Mg(Zn)$  at cube corners,  $Ni$  at the faces and  $C$  at the octahedral interstitial site, the total energy minimization were carried out to determine the equation of state parameters. The total energies calculated, self-consistently, for six lattice constants close to equilibrium were fed as input to a third-order Birch-Murnaghan equation of state [38, 39]. Note that the Birch-Murnaghan equation is derived from the theory of finite strain, by considering an elastic isotropic medium under isothermal compression, with the assumption that the pressure-volume relation remains linear. Hence, in the optimization procedure we have restricted the choice close to the equilibrium.

	GGA		LDA	
	$ZnCNi_3$	$MgCNi_3$	$ZnCNi_3$	$MgCNi_3$
$a_{eq}$ (a.u.)	7.2255	7.3041	7.0558	7.1387
$B_{eq}$ (Mbar)	0.3886	0.3479	0.4656	0.4188
$B'_{eq}$	4.4106	4.5255	4.3444	4.7813

**Table 2.** Comparison of the equation of state parameters of cubic perovskite  $ZnCNi_3$  with that of  $MgCNi$  using the KKR-ASA method as described in the text.

Since the choice of the exchange correlation potential in the Kohn-Sham Hamiltonian has proven to be sensitive in the structural characterization, we have carried

out the total energy minimization for two different approximations, namely the LDA and GGA [32, 33]. The results are shown in Table.2. The GGA considerably overestimates the lattice constant for either alloys, when compared to the experimental values. For  $MgCNi_3$ , using the LDA description of the exchange-correlation, the lattice constant was calculated as 7.139 a.u., with the bulk modulus and its pressure derivative as 0.42 Mbar and 4.78 respectively. These values are consistent with the earlier first-principles reports [4, 6]. The underestimation in the lattice constant for  $MgCNi_3$ , however when compared to the experiments, owe to the over-binding effects in the LDA, and is a well known problem.

For  $ZnCNi_3$  the equilibrium lattice constant calculated using LDA yielded the value as 7.056 a.u. which when compared to the recent X-ray diffraction results [2] of 6.918 a.u., was found to be an overestimation. However, the results of the present calculations are consistent with the works of Johannes and Pickett [3] who employed the FP-LAPW method. Note that the consistency of the ASA calculations with that of the full-potential counterparts owe to the inclusion of the muffin-tin correction [28]. The KKR-ASA calculations further finds the bulk modulus and its pressure derivative of  $ZnCNi_3$  as 0.46 Mbar and 4.34, respectively. As mentioned above, the overestimation of lattice constant in LDA is not so common, which suggests that the samples subjected to the experiments may be sub-stoichiometric. This was also emphasized by Johannes and Pickett [3] following the crystal structure characterization of  $MgC_yNi_3$  alloys [8]. In the latter, both experiments [8, 12] and theoretical calculations [13] have shown that the lattice constant decreases as the  $C$  content in the material decreases.

To look for the changes in the equation of state parameters as a function of  $C$  content in  $MgC_yNi_3$  and  $ZnC_yNi_3$  alloys, total energy minimization was carried out. The variation is shown in Fig.1. For both  $MgC_yNi_3$  and  $ZnC_yNi_3$  alloys, the lattice constant as well as the bulk modulus decrease as  $C$  at% decreases. For  $MgC_yNi_3$  observed trend is consistent with the earlier X-ray diffraction measurements. The rate of decrease in the lattice constant is estimated as 0.142 a.u./at% $C$  while for  $ZnC_yNi_3$ , the lattice constant was found to decrease at the rate of 0.189 a.u. per at% of  $C$ . Though the lattice constant and bulk modulus showed similar trend for either alloys, the change in the pressure derivative of the bulk modulus as a function of  $y$  characteristically differed.

The pressure derivative of the bulk modulus measures the rate at which the material becomes incompressible with increasing pressure, and is sensitive to the softness of the equation of state. In the Debye approximation for isotropic solids, which assumes a uniform dependence of the lattice frequencies with volume, one may express the average phonon frequency  $\omega$  as  $B'_{eq} \propto \frac{\delta \ln \omega}{\delta \ln V}$ , where  $V$  is the equilibrium volume of the unit cell. Note that volume for the vacancy-rich alloys decreases with decreasing  $y$ , while  $B'_{eq}$  maps a different trend for  $MgC_yNi_3$  and  $ZnC_yNi_3$  alloys. Such a behaviour indicates that the properties associated with the  $MgC_yNi_3$  lattice could be characteristically different from that of the  $ZnC_yNi_3$  counterparts. Also, one may note that the phonon spectrum for  $MgCNi_3$  reveals that certain  $C$  modes play a vital role in the materials

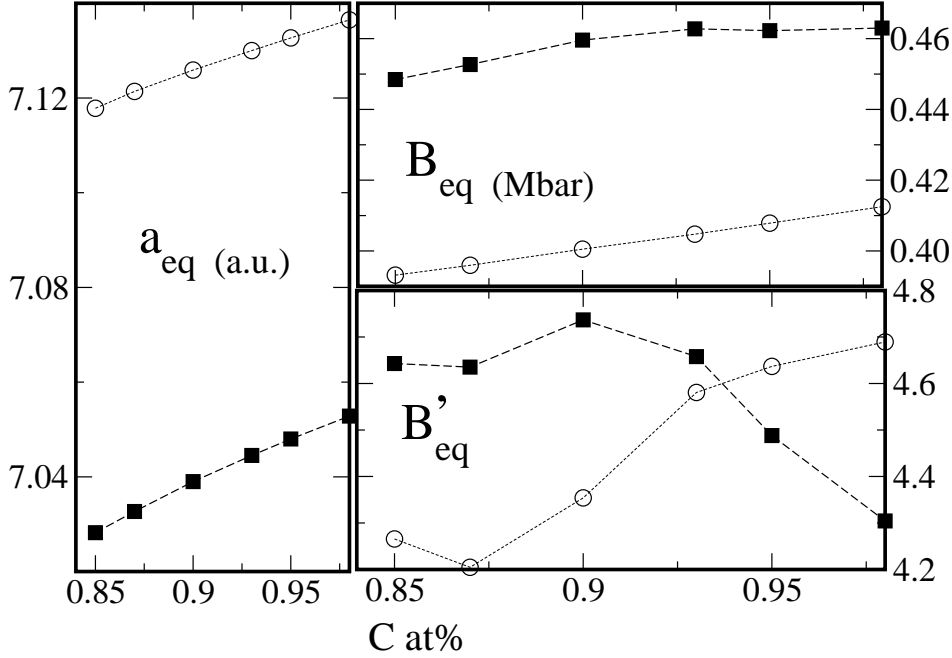


**Figure 1.** The variation in the equation of state parameters, equilibrium lattice constant  $a_{eq}$  (a.u.) , the bulk modulus  $B_{eq}$  (Mbar) and the pressure derivative of the bulk modulus, as a function of  $y$  in  $MgC_yNi_3$  (open circles) and  $ZnC_yNi_3$  (filled squares) calculated using the KKR-ASA-CPA method as described in the text.

superconducting properties in addition to those of the  $Ni$  modes [40, 41].

Partial replacement of  $Zn$  for  $Mg$  in  $MgCNi_3$  has shown that the transition temperature decreases [42]. The findings also conclude that the nature of pairing mechanism in  $MgCNi_3$  is conventional [42]. To study the changes brought about by  $Zn$  substitutions in the  $Mg$  sub-lattice of  $MgCNi_3$ , we have carried out KKR-ASA-CPA calculations for  $Mg_{1-x}Zn_xNi_3$  alloys. In Fig.2, we show the variation of the equation of state parameters of  $Mg_{1-x}Zn_xNi_3$  alloys. The decrease in the lattice constant is consistent with the previous experimental report. The bulk modulus as well as its pressure derivative increases as  $x$  increases in  $Mg_{1-x}Zn_xNi_3$  alloys. This clearly indicates that the average phonon frequency gets modulated as  $Zn$  replaces  $Mg$  in  $MgCNi_3$ .

### 3.2. Electronic structure

In Fig.3, we show the total and sub-lattice resolved partial densities of states of  $MgCNi_3$  and  $ZnCNi_3$  calculated at their respective equilibrium lattice constants. The characteristic features of both  $MgCNi_3$  and  $ZnCNi_3$  appear more or less similar with an exception of a sharp peak in the energy range  $-0.6 \leq E \leq -0.4$ , characteristic of  $Zn$  3d states. Being deep below on the energy scale compared to the Fermi energy, which is zero on the scale shown, one may expect  $Zn$  d states to be localized and thus behave

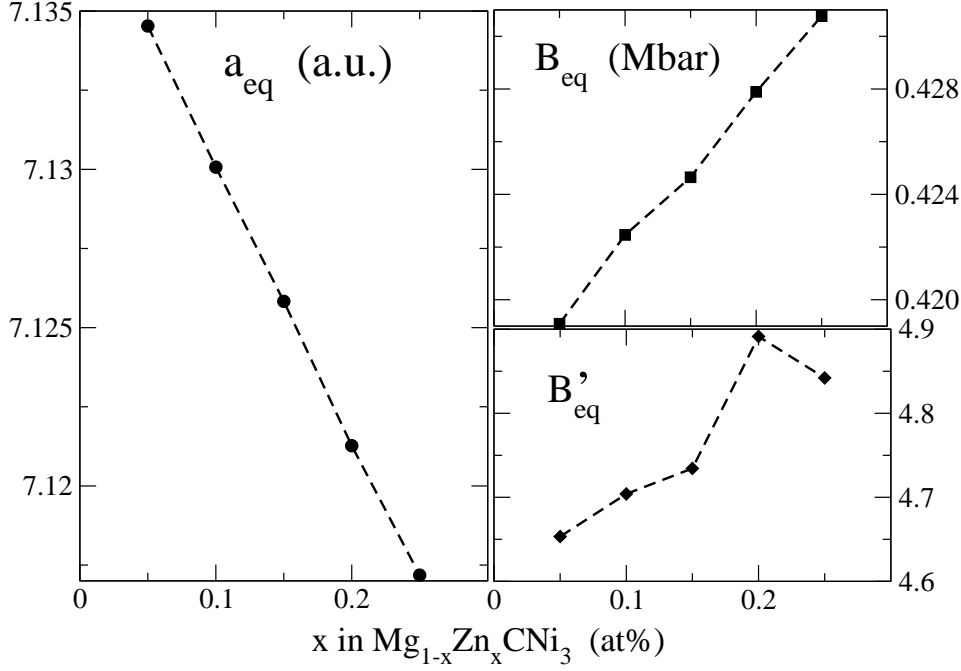


**Figure 2.** The variation in the equation of state parameters, equilibrium lattice constant  $a_{eq}$  (a.u.), the bulk modulus  $B_{eq}$  (Mbar) and the pressure derivative of the bulk modulus, as a function of  $x$  in  $Mg_{1-x}Zn_xCNi_3$  calculated using the KKR-ASA-CPA method as described in the text.

atomically. While for  $MgCNi_3$  a small peak characteristic of the  $Mg-Ni$  bonding also appears in this energy range, but is less pronounced. Furthermore, the states near  $E_F$  are predominantly  $Ni$   $3d$  in character in both alloys, with little admixture of the  $C$   $2p$  states. One may also find that the position of the  $Ni$   $3d$  derived singularity is slightly lower in the energy scale for  $ZnCNi_3$  than for  $MgCNi_3$ , which is consistent with the previous results. The  $N(E_F)$  and the contributions to it from the sub-lattices are compared in Table.4.

	$N(E_F)$	$Zn(Mg)$	$C$	$Ni$	$Ni d_{xy(xz)}$	$Ni d_{yz}$	$Ni d_{x^2-y^2}$	$Ni d_{3z^2-1}$
$ZnCNi_3$	13.005	0.945	1.076	10.984	4.002	0.168	1.296	0.606
$MgCNi_3$	14.557	1.016	1.199	12.341	4.509	0.097	1.474	0.658

**Table 4.** Comparison of the total  $N(E_F)$  and sub-lattice resolved density of states of  $ZnCNi_3$  and  $MgCNi_3$  expressed in units of states/Ry atom.

The reported values of  $N(E_F)$  for  $MgCNi_3$  are at variance with the existing reports [4, 5, 6, 7, 43, 44, 45, 46, 47]. It appears that the value is sensitive to the basic approximations made in each type of the electronic structure method, and also to the parameters like that of the choice of Wigner-Seitz radii, choice of the exchange-correlation potential and others. However, under similar approximations, it is clear that for  $ZnCNi_3$  the  $N(E_F)$  reduces by 12% in comparison with  $MgCNi_3$ . This is consistent with the earlier first-principles FP-LAPW calculations [3]. The reduction in  $N(E_F)$  may be largely due to the smaller lattice constant of  $ZnCNi_3$ , in comparison



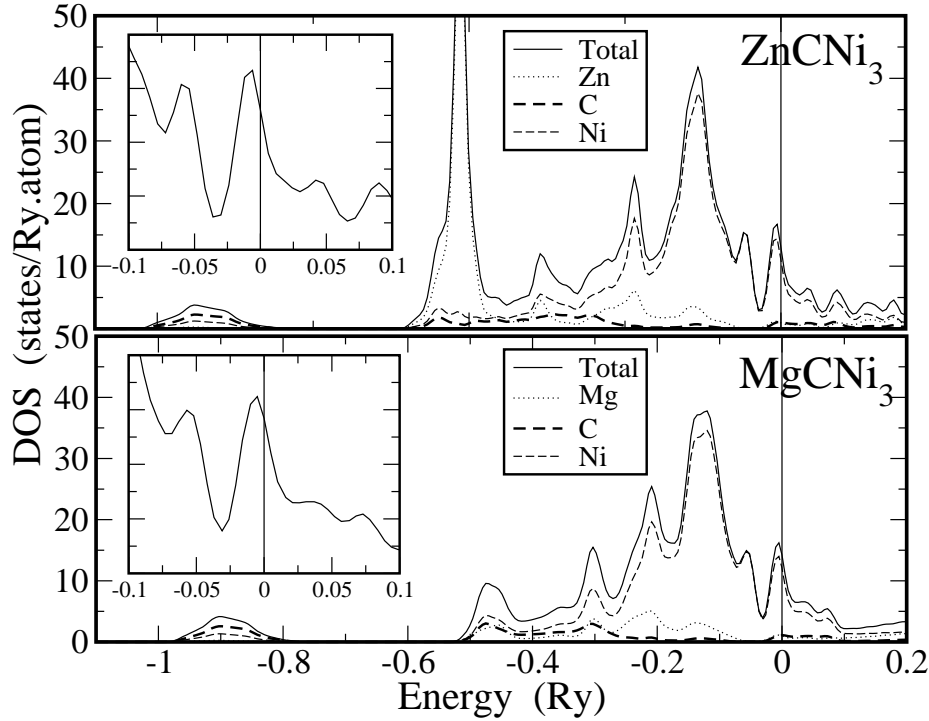


**Figure 3.** Comparison of the total and sub-lattice resolved partial density of states of  $ZnCNi_3$  and  $MgCNi_3$ , calculated at their respective equilibrium lattice constants. The vertical line through energy zero represents the alloy Fermi energy. In the inset we show a blow up of the total density of states near the Fermi energy.

more significant in  $MgCNi_3$  when compared to  $ZnCNi_3$ . This is consistent with the fact that a larger fraction of the charge would be transferred back to the  $Mg$  sub-lattice, in  $MgCNi_3$  in comparison with that of the  $Ni$  sub-lattice.

The change in the  $N(E_F)$  as a function of lattice constant in  $Mg_{1-x}Zn_xCNi_3$  alloys is shown in Fig.9. One may find that  $N(E_F)$  decreases for all values of  $x$ , with respect to lattice constant. However,  $N(E_F)$  as a function of  $x$ , at the equilibrium lattice constant, was found to deviate a little, as is evident from Fig.9. This clearly suggests that the electronic structure properties are mainly governed by the  $CNi_6$  octahedra. The atoms occupying the cube corners i.e.,  $Mg$  and  $Zn$ , however, play a non-trivial role in determining the structural properties.

### 3.3. Hopfield parameter

The Hopfield parameter  $\eta$  has been regarded as a local “chemical” property of an atom in a crystal. It has been emphasized earlier that the most significant single parameter in understanding the  $T_C$  of a conventional superconductor is the Hopfield parameter [35]. For strong-coupling systems, the variation in  $\eta$  is more important than the variation of  $\langle\omega^2\rangle$  in changing  $T_C$ . Softening  $\langle\omega^2\rangle$  often does enhance  $T_C$ , but a significant change in the magnitude of  $T_C$  depends largely on a significant change in the  $\eta$  value rather

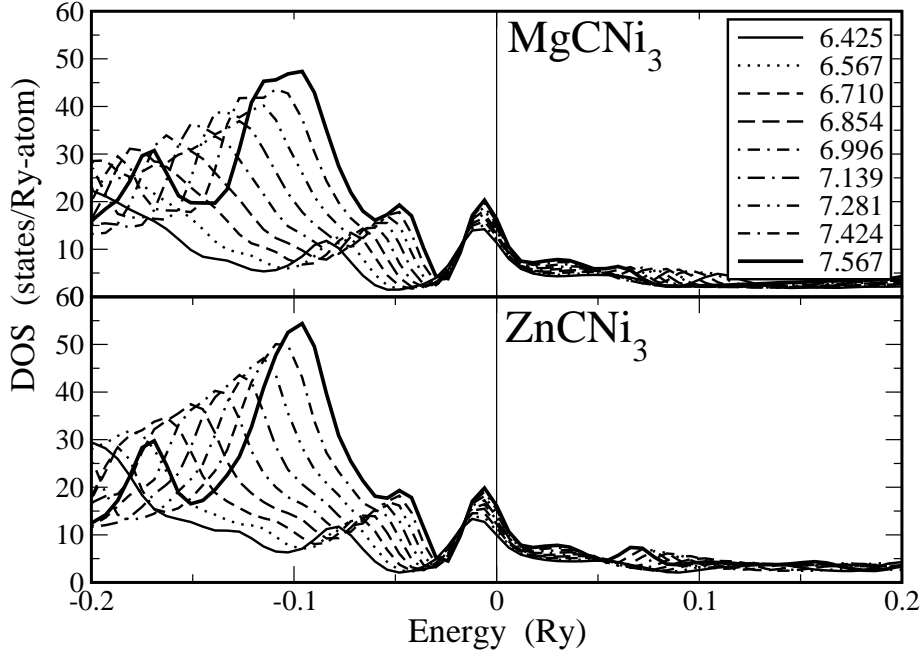


**Figure 4.** Comparison of the change in the total density of states near Fermi energy of  $ZnCNi_3$  and  $MgCNi_3$  for a range of lattice constant as indicated in the figure. The vertical line through energy zero represents the alloy Fermi energy.

than a small change in the corresponding  $\langle\omega^2\rangle$ . As a matter of fact, we look for the changes in the  $\eta$  from the three sub-lattices of these perovskites as a function of lattice constant as well as  $y$  in  $MgC_yNi_3$  and  $ZnC_yNi_3$  alloys. Note that for  $MgCNi_3$ , it has been reported that the superconducting transition temperature  $T_C$  increases upon application of external pressure [48, 49]. Besides, experiments remain controversial on the strength of the electron-phonon interaction in  $MgCNi_3$  [50, 51, 48, 52]. It has been suggested that  $MgCNi_3$  may be a strongly-coupled superconductor, however, the magnitude of  $T_C$  being marginally reduced due to the paramagnon interactions [4, 51].

In Fig.10 we show the changes in the  $\eta$  of  $MgCNi_3$  and  $ZnCNi_3$  as a function of lattice constant. It is clear from Fig.10 that the  $\eta_C$  and  $\eta_{Ni}$  linearly increase as a function of decreasing volume in either alloys. If the change in the average phonon frequency remains small, then either of these alloys could enhance the transition temperature with respect to external pressure. For  $MgCNi_3$  this view is consistent with the previous experimental results. Similar characteristic feature holds for the vacancy-rich disordered alloys, the variation of which is shown in Fig.11 and 12

To have an understanding in the variation of  $\eta_C$ ,  $\eta_{vac}$  and  $\eta_{Ni}$  where  $\eta_{vac}$  can be considered as the local chemical property of the electrons in the empty sphere, we show in Fig.13 the change in these parameters as a function of  $y$  in both  $MgC_yNi_3$  and  $ZnC_yNi_3$  alloys. One may find that the variation of  $\eta$  remains similar for both the alloys as a function of decreasing  $C$  content.

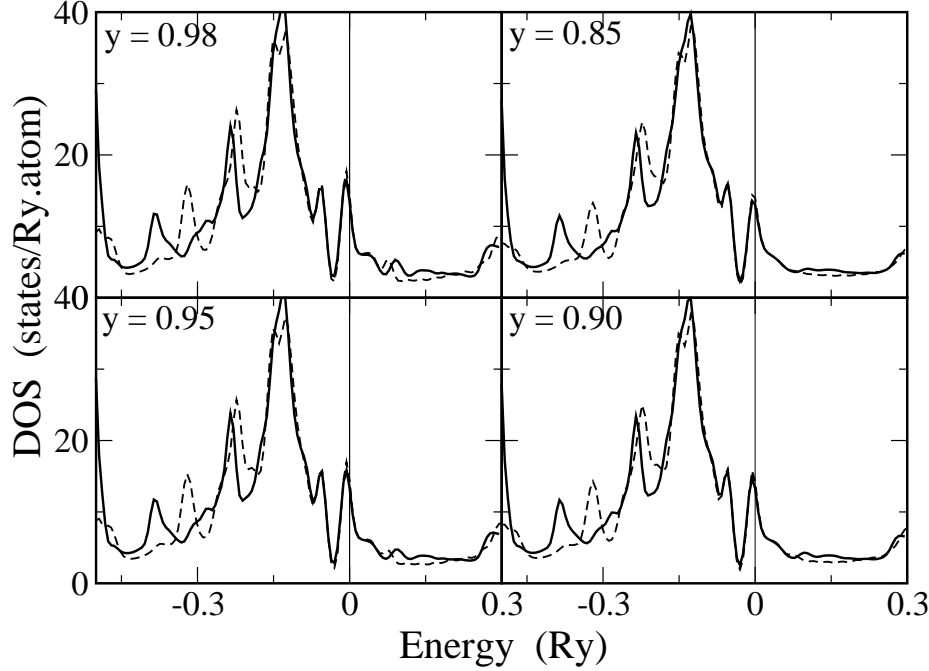


**Figure 5.** Comparison of the change in the total density of states of  $ZnC_yNi_3$  (solid line) and  $MgC_yNi_3$  (dashed lines) alloys calculated at their equilibrium lattice constant with  $y$  as indicated. The vertical line through energy zero in each panel shows the Fermi energy.

### 3.4. Magnetic properties

Total energies from both the self-consistent, spin polarized and spin unpolarized calculations remain degenerate for  $MgCNi_3$  and  $ZnCNi_3$  alloys at their equilibrium lattice constants. This unambiguously shows that the materials are non-magnetic in nature. However, having suggested that  $MgCNi_3$  is on the verge of a ferromagnetic instability [4, 5, 51, 53, 54], and also that incipient magnetism in the form of spin-fluctuations reside in the material, we attempt to compare the magnetic properties of  $MgCNi_3$  and  $ZnCNi_3$  alloys using the fixed-spin moment approach of alloy theory [25].

Numerical calculations of magnetic energy  $\Delta E(M)$  for  $MgCNi_3$  and  $ZnCNi_3$  are carried out over a range of lattice constants. The calculated results of  $\Delta E(M)$  in the fixed-spin-moment method are shown in Fig.14. The calculated  $\Delta E(M)$  curves are fit to the form of a power series of  $M^{2n}$  up to  $n = 3$ , for the polynomial as mentioned above. The variations of the coefficients,  $a_2$  in units of  $\frac{T}{\mu_B}$ ,  $a_4$  in  $\frac{T^3}{\mu_B^3}$ , and  $a_6$  in  $\frac{T^5}{\mu_B^5}$  as a function of lattice constant are shown in Fig.15. The propensity of magnetism can be inferred from the sign of the coefficient which is quadratic in  $M$ , i.e.,  $a_2$ . The coefficient  $a_2$  is the measure of the curvature and is positive definite when the total energy minimum is at  $M = 0$ , thus referring to a paramagnetic ground state. In general, when  $a_2$  becomes negative, it infers that there would exist a minimum in the  $\Delta E - M$  curve at a value other than  $M = 0$  referring to a ferromagnetic phase at that value of  $M$ . The higher-

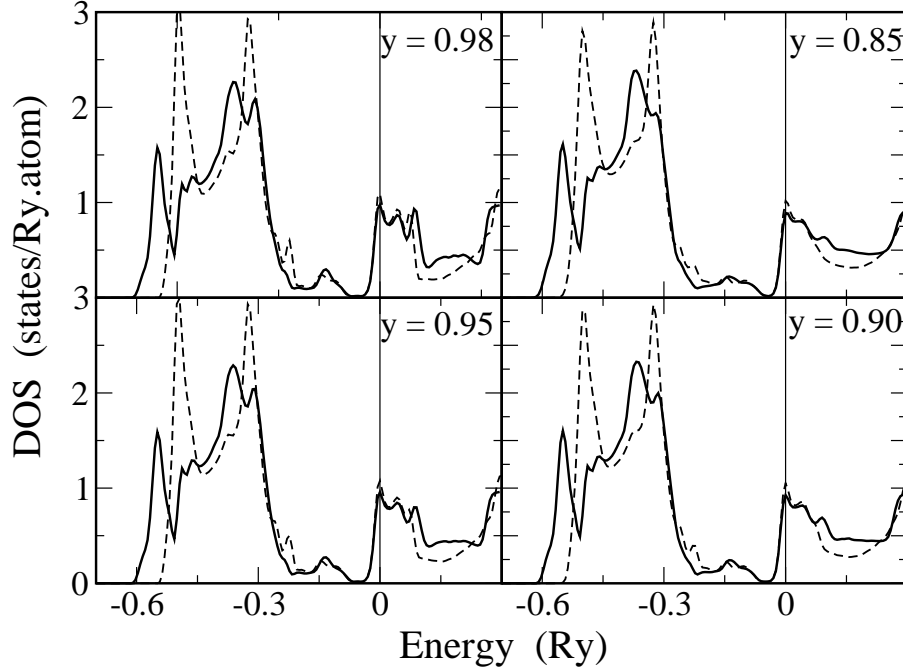


**Figure 6.** Comparison of the change in the sub-lattice resolved  $C$   $2p$  partial density of states of  $ZnC_yNi_3$  (solid line) and  $MgC_yNi_3$  (dashed lines) alloys calculated at their equilibrium lattice constant with  $y$  as indicated. The vertical line through energy zero in each panel represents the Fermi energy.

order coefficients  $a_4$  and  $a_6$  however are significant and they control the variation of  $\Delta E$  with respect to  $M$ . For example, for larger values of  $M$ ,  $a_4$  and successively  $a_6$  would dominate, and if  $a_4(a_6)$  tends to be negative it would show a dip in the  $\Delta E - M$  variation pointing towards a magnetic transition at a higher value of  $M$ . This, in the first-principles characterization of the magnetic properties of a material would refer to a possibility of a metastable phase at relatively large values of external magnetic fields. However, it has to be noted that calculations for large values of  $M$  can result in ambiguous results. Hence, it is suggested to carry out calculations for smaller values of  $M$  and use the above mentioned polynomial function up to the minimum order, where the curve fits with sufficient accuracy.

Fig. 15 shows that for smaller values of lattice constant, the alloys show an enhanced paramagnetic character. One may also note that the variation in  $a_4$  and  $a_6$  coefficients are oppositely complimented and hence in the renormalized approach to include corrections due to spin-fluctuations, as suggested by Yamada and Terao [55], they would cancel out in proportion preserving the trend in the variation of  $a_2$ . Thus, it becomes likely that the incipient magnetic properties associated with  $MgCNi_3$  and  $ZnCNi_3$  would decrease as a function of decreasing lattice constant.

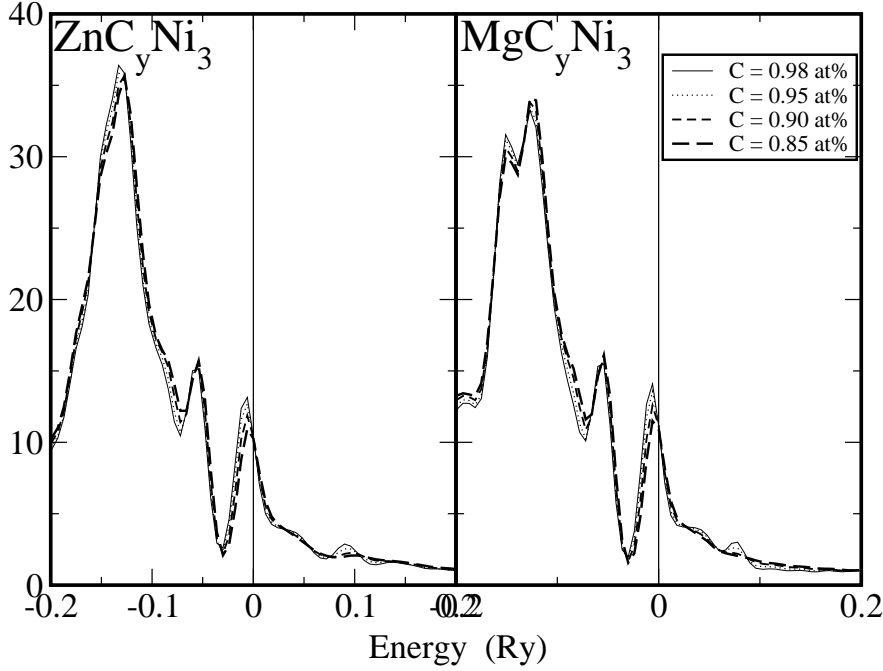


**Figure 7.** Comparison of the change in the sub-lattice resolved  $Ni$   $3d$  partial density of states of  $ZnC_yNi_3$  and  $MgC_yNi_3$  alloys, over a small energy window around Fermi energy, calculated at their equilibrium lattice constant with  $y$  as indicated. The vertical line through energy zero in each panel represents the Fermi energy.

#### 4. Conclusions

First-principles study of the electronic properties of  $MgCNi_3$  and  $ZnCNi_3$ , and also their non-stoichiometric alloys are carried out using the density-functional-based KKR-ASA method. We find that the lattice constant for  $ZnCNi_3$  is overestimated, while for  $MgCNi_3$  it is underestimated. This suggests that the material  $ZnCNi_3$  subjected to experiments may be non-stoichiometric. As a function of decreasing  $C$  content in  $MgC_yNi_3$  and  $ZnC_yNi_3$  alloys, one finds an opposite trend in the variation of pressure derivative of the bulk modulus, which is proportional to the averaged phonon frequency. With electronic structure remaining essentially the same for  $MgC_yNi_3$  and  $ZnC_yNi_3$ , the results hint that non-stoichiometry may have opposite effects. Note that for  $0.9 < y < 1.0$ ,  $MgC_yNi_3$  alloys are feebly superconducting, while according to the conjecture that has been made  $ZnC_yNi_3$  is not. It can thus be inferred that the associated phonon modes in  $ZnCNi_3$  and its disordered alloys may be characteristically different when compared to the  $MgCNi_3$  counterparts. A comparison of the phonon spectra of these alloys thus become quite necessary to understand the absence of superconductivity in  $ZnCNi_3$ , although it is iso-structural and iso-valent with  $MgCNi_3$ .

[1] T. He, K.A. Regan, M.A. Hayward, A.P. Ramirez, Y. Wang, P. Khalifah, T. He, J.S. Slusky, N. Rogado, K. Inumaru, M.K. Haas, H.W. Zandbergen, N.P. Ong, and R.J. Cava, *Nature*, 411, 54 (2001)

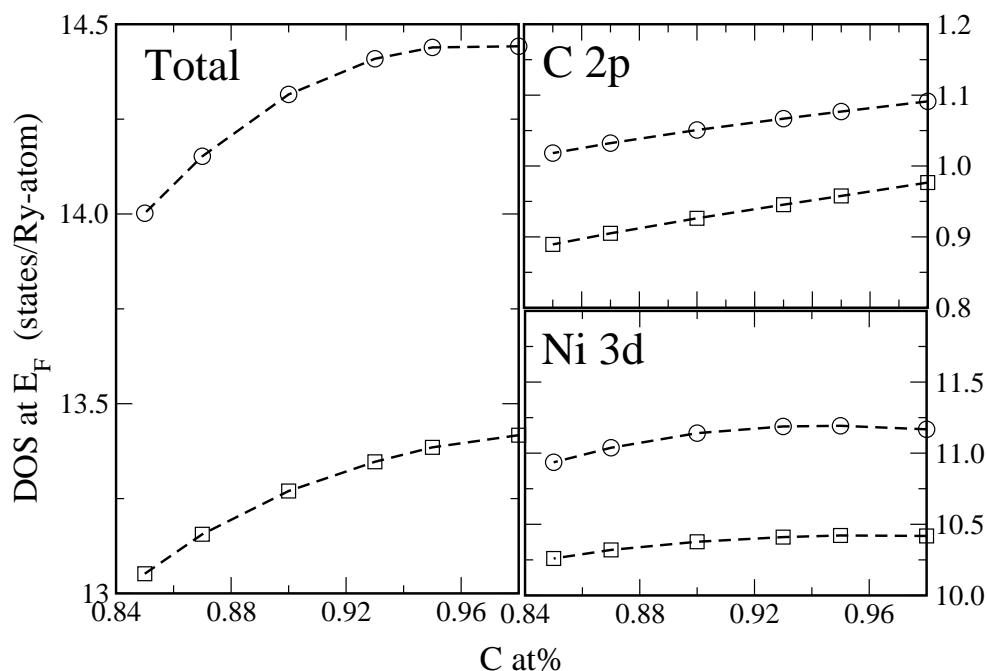


**Figure 8.** Comparison of the change in the total, sub-lattice resolved  $C$  2p and  $Ni$  3d partial densities of states at  $E_F$  of  $ZnC_yNi_3$  (squares) and  $MgC_yNi_3$  (circles) as a function of  $y$ .

- [2] M.- S. Park, J. Giim, S. H. Park, H. C. Ri, S. I. Lee, and E. J. Choi, Supercond. Sci. Technol. 17, 274 (2004).
- [3] M. D. Johannes and W. E. Pickett, Phys. Rev. B 70, 060507 (2004)
- [4] D. J. Singh and I. I. Mazin, Phys. Rev. B 64, 140507 (2001)
- [5] H. Rosner, R. Weht, M. D. Johannes, W. E. Pickett, and E. Tosatti, Phys. Rev. Lett. 88, 027001 (2002)
- [6] S. B. Dugdale and T. Jarlborg, Phys. Rev. B 64, 100508 (2001)
- [7] Szajek A, J. Phys.: Condens. Matter 13, L595 (2001)
- [8] A. Ren, G. C. Che, S. L. Jia, H. Chen, Y. M. Ni, G. D. Liu and Z. X. Zhao, Physica C 371, 1 (2002)
- [9] J. Q. Li, L. J. Wu, L. Li, and Y. Zhu, Phys. Rev. B 65, 052506 (2002)
- [10] J. H. Kim, J. S. Ahn, J. Kim, M.-S. Park, S. I. Lee, E. J. Choi, and S.-J. Oh, Phys. Rev. B 66, 172507 (2002)
- [11] G. Kinoda, M. Nishiyama, Y. Zhao, M. Murakami, N. Koshizuka and T. Hasegawa, Japan. J. Appl. Phys. 40 L1365, (2001)
- [12] L. Shan, K. Xia, Z. Y. Liu, H. H. Wen, Z. A. Ren, G. C. Che and Z. X. Zhao, Phys. Rev. B 68 024523 (2003)
- [13] P. J. T. Joseph and P. P. Singh, Phys. Rev. B 72, 064519 (2005)
- [14] P. J. T. Joseph and P. P. Singh, Phys. Rev. B 72, 214206 (2005)
- [15] H. H. Stadelmaier and L. J. Huetter, Z. Metallk 50, 199 (1959)
- [16] H. H. Stadelmaier and L. J. Huetter, Acta Metall., 7, 415 (1959)
- [17] H. H. Stadelmaier and F. H. Hammad, Metall 15, 124 (1961)
- [18] T.G. Amos, Q. Huang, J.W. Lynn, T. He, R.J. Cava, Solid State Commun 121, 73 (2002)
- [19] H. H. Stadelmaier and T. S. Yun, Z. Metallk 52, 477 (1961)
- [20] J. B. Goodenough and J. M. Longo, Landolt- Bornstein series, Vol IIIa
- [21] J. Koringa, Physica 13, 392 (1947)

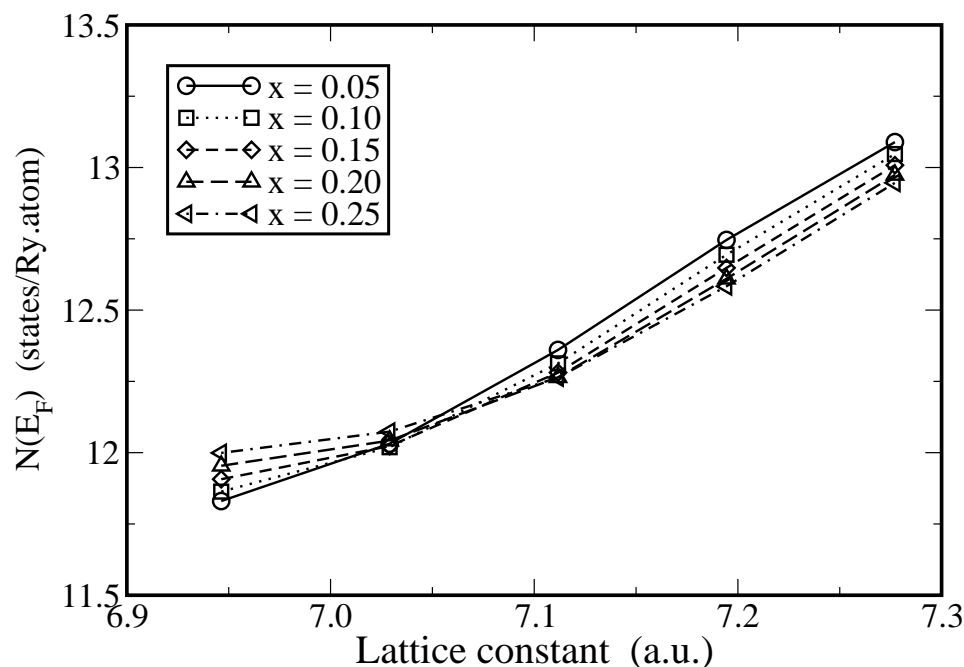


**Figure 9.** The change in the total density of states at the Fermi energy,  $N(E_F)$ , in units of states/Ry atom as a function of lattice constant in  $Mg_{1-x}Zn_xCNi_3$  alloys. The values of  $x$  are as shown in the figure.

- [22] W. Kohn and N. Rostoker, Phys. Rev 94, 1111 (1954)
- [23] I. Turek, V. Drchal, J. Kudrnovsky, M. Sob and P. Weinberger, Electronic Structure of Disordered Alloys, Surfaces and Interfaces, Kluwer Academic Publishers, 1997.
- [24] P. Soven Phys. Rev. 156, 809 (1967)
- [25] K Schwarz and P Mohn, J. Phys. F: Met. Phys. 14, L129 (1984)
- [26] Statistical Physics, L. D. Landau and E. M. Lifshitz, Pergamon press London (1962)
- [27] H. L. Skriver and I. Mertig, Phys. Rev. B 32, 4431 (1985)
- [28] N. E. Christensen and S. Satpathy, Phys. Rev. Lett. 55, 600 (1985).
- [29] A. V. Ruban and H. L. Skriver Phys. Rev. B 66, 024201 (2002)
- [30] A. V. Ruban, S. I. Simak, P. A. Korzhavyi, and H. L. Skriver Phys. Rev. B 66, 024202 (2002)
- [31] A. V. Ruban and H. L. Skriver Computational Materials Science, 15, 119 (1999)
- [32] J. P. Perdew and Y. Wang, Phys. Rev. B 45, 13244 (1992).
- [33] J. P. Perdew, K. Burke, and Y. Wang, Phys. Rev. B 54, 16533 (1996)
- [34] Hans. L. Skriver, The LMTO method, Muffin tin orbitals and electronic structure, Springer- Verlag (1984)
- [35] Superconductivity in  $d$ - and  $f$ - band metals, edited by D. H. Douglass, Plenum press NewYork (1976)
- [36] G. D. Gaspari and B. L. Gyorffy, Phys. Rev. Lett. 28, 801 (1972)
- [37] R. Hayn and V. Drchal Phys. Rev. B 58, 4341 (1998)
- [38] F. Birch, J. Geophys. Res. 57, 227 (1952)
- [39] F. D. Murnaghan, Wiley, New York, 140 pp. (1951)
- [40] R. Heid, B. Renker, H. Schober, P. Adelmann, D. Ernst, and K.-P. Bohnen, Phys. Rev. B 69, 092511 (2004)
- [41] A. Yu. Ignatov, S. Y. Savrasov, and T. A. Tyson, Phys. Rev. B 68, 220504 (2003)
- [42] S. -H. Park, Y. W. Lee, J. Giim, Sung-Hoon Jung, H. C. Ri and E. J. Choi, Physica C 400, 160

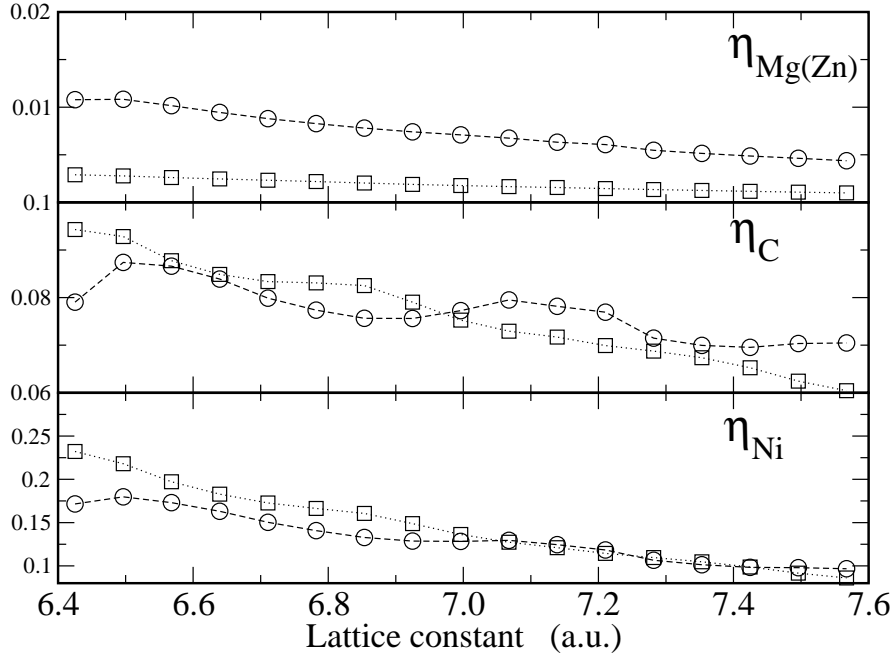


**Figure 10.** Comparison of the change in the  $\eta_{Mg/Zn}$ ,  $\eta_C$  and  $\eta_{Ni}$  as a function of lattice constant of  $MgCNi_3$  (circles) and  $ZnCNi_3$  (squares).

(2004)

- [43] I. R. Shein, A. L. Ivanovskii, E. Z. Kurmaev, A. Moewes, S. Chiuzbian, L. D. Finkelstein, M. Neumann, Z. A. Ren, and G. C. Che, Phys. Rev. B 66, 024520 (2002)
- [44] I. G. Kim, J. I. Lee and A. J. Freeman, Phys. Rev. B 65, 064525 (2002)
- [45] X. Zheng, Y. Xu, Z. Zeng and E. Baggio-Saitovitch, Physica C 408-410, 154 (2004)
- [46] M. Q. Tan, X. M. Tao, X. J. Xu, J. H. He and G. X. Ye, Physica B 337, 95 (2003)
- [47] J. L. Wang, Y. Xu, Z. Zeng, Q. Q. Zheng, H. Q. Lin, J. Appl. Phys 91, 8504 (2002)
- [48] H. D. Yang, S. Mollah, W. L. Huang, P. L. Ho, H. L. Huang, C. J. Liu, J. Y. Lin, Y. L. Zhang, R. C. Yu and C. Q. Jin, Phys. Rev. B 68 092507 (2003)
- [49] T. G. Kumary, J. Janaki, A. Mani, S. M. Jaya, V. S. Sastry, Y. Hariharan, T. S. Radhakrishnan, and M. C. Valsakumar, Phys. Rev. B 66, 064510 (2002)
- [50] J.-Y. Lin, P. L. Ho, H. L. Huang, P. H. Lin, Y.-L. Zhang, R.-C. Yu, C.-Q. Jin, and H. D. Yang Phys. Rev. B 67, 052501 (2003)
- [51] A. Walte, G. Fuchs, K.-H. Muller, A. Handstein, K. Nenkov, V. N. Nazhny, S.-L. Drechsler, S. Shulga, L. Schultz, and H. Rosner Phys. Rev. B 70, 174503 (2004)
- [52] Z. Q. Mao, M. M. Rosario, K. D. Nelson, K. Wu, I. G. Deac, P. Schiffer, Y. Liu, T. He, K. A. Regan, and R. J. Cava Phys. Rev. B 67, 094502 (2003)
- [53] L. Shan, Z. Y. Liu, Z. A. Ren, G. C. Che, and H. H. Wen, Phys. Rev. B 71, 144516 (2005)
- [54] P. M. Singer, T. Imai, T. He, M. A. Hayward, and R. J. Cava, Phys. Rev. Lett. 87, 257601 (2001)
- [55] H. Yamada and K. Terao, Phys. Rev. B 59, 9342 (1999)



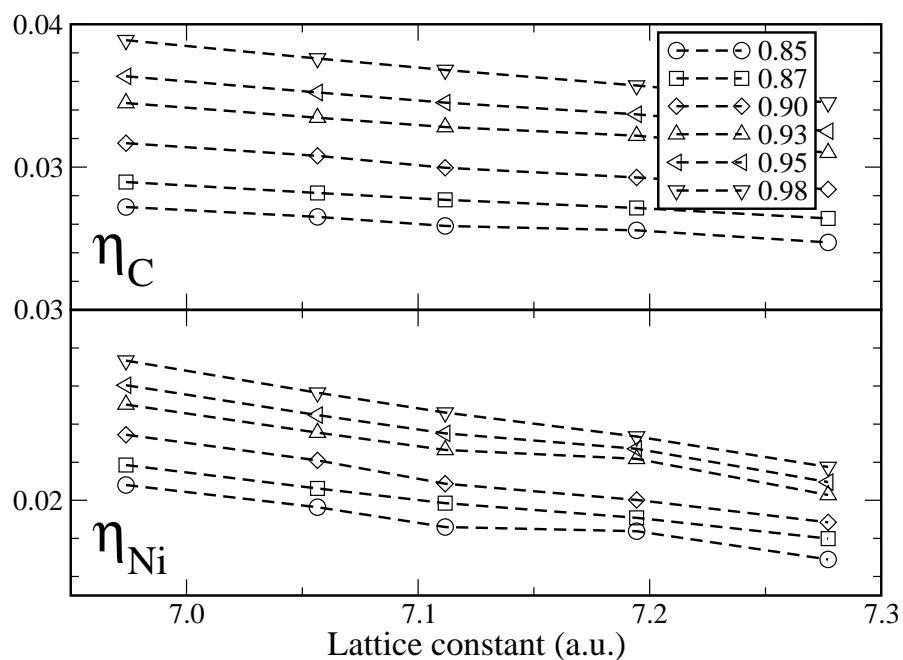


**Figure 11.** The change in the  $\eta_C$  (upper panel) and  $\eta_{Ni}$  (lower panel) as a function of lattice constant in  $MgC_yNi_3$  alloys with  $y$  as indicated.

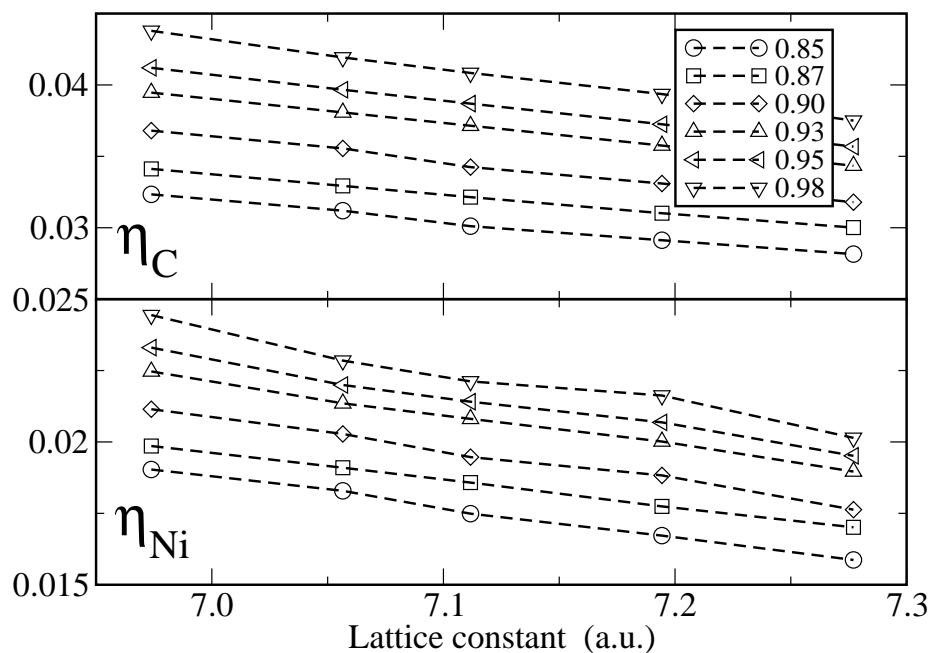


**Figure 12.** The change in the  $\eta_C$  (upper panel) and  $\eta_{Ni}$  (lower panel) as a function of lattice constant in  $ZnC_yNi_3$  alloys with  $y$  as indicated.

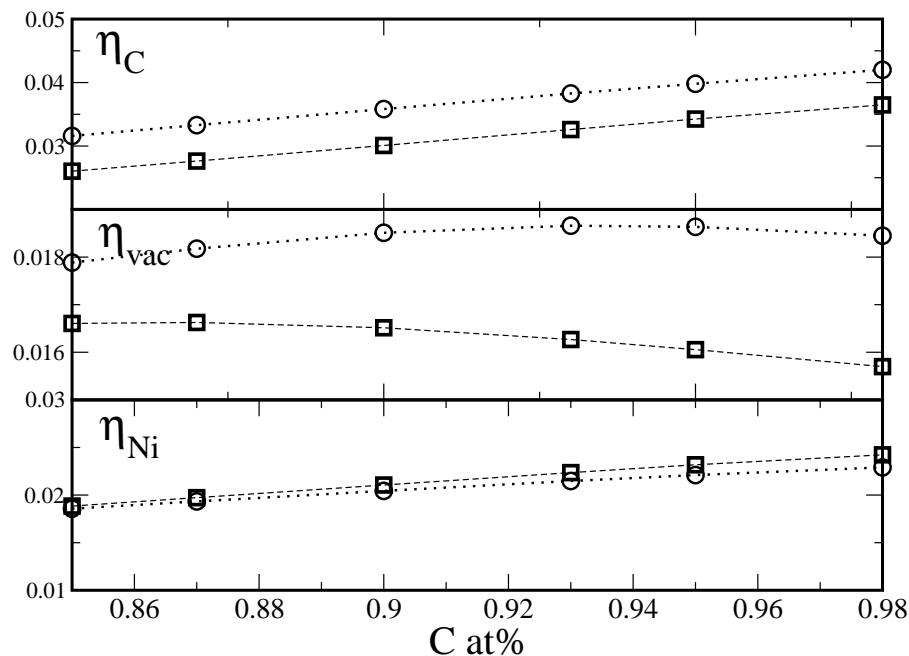


**Figure 13.** Comparison of the change in the  $\eta_C$ ,  $\eta_{vac}$  and  $\eta_{Ni}$  as a function of  $y$  in  $ZnC_yNi_3$  (squares) and  $MgC_yNi_3$  (circles) alloys.

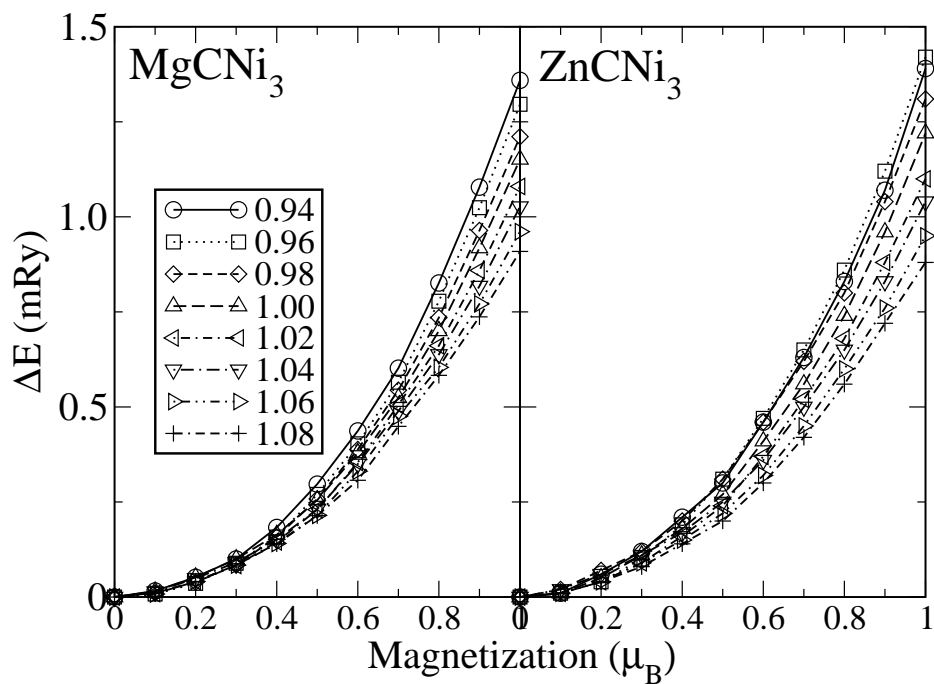


**Figure 14.** Comparison of the change in the magnetic energy as a function of magnetization in  $MgCNi_3$  and  $ZnCNi_3$  alloys for a range of lattice constant ratio  $a/a_{eq}$ , where  $a_{eq}$  is the equilibrium lattice constant of the respective alloys.

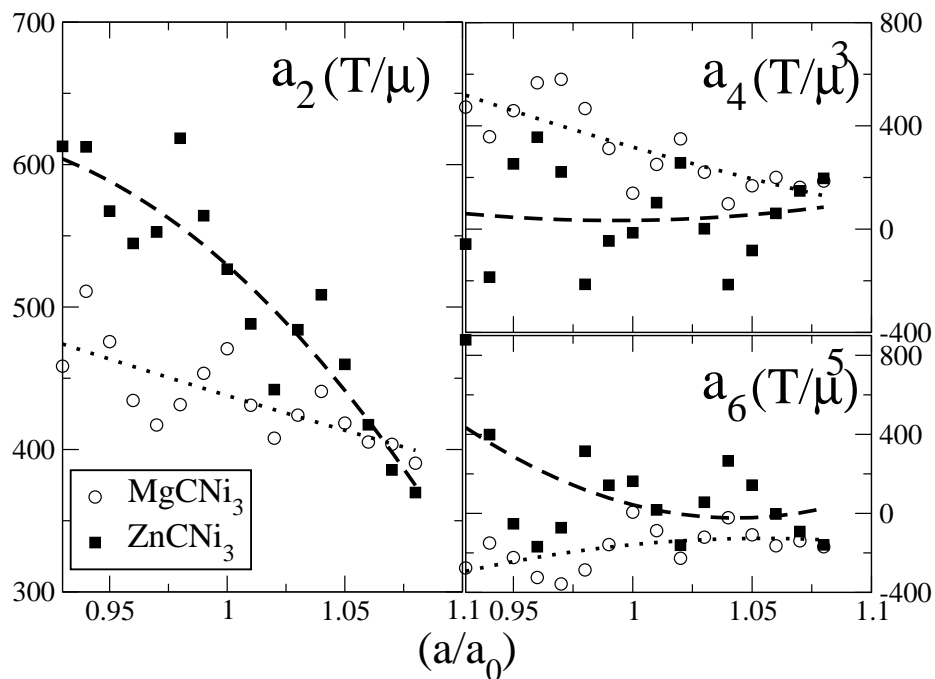


**Figure 15.** Comparison of the changes in the Landau coefficients  $a_2$ ,  $a_4$  and  $a_6$  as a function lattice constant in  $MgCNi_3$  and  $ZnCNi_3$  alloys. The open circles and filled squares are the calculated values and the best quadratic fit representing these points are shown with dotted and dashed lines, respectively for  $MgCNi_3$  and  $ZnCNi_3$  alloys.